IEEE Access
Multidisciplinary | Rapid Review | Open Access Journal

Received June 7, 2021, accepted June 23, 2021, date of publication June 29, 2021, date of current version July 13, 2021.

Digital Object Identifier 10.1109/ACCESS.2021.3093482

An Ultrasonic Signal Denoising Method for EMU Wheel Trackside Fault Diagnosis System Based on Improved Threshold Function

ZHILIN SUN[1,2] **AND JINGUI LU**[1]
[1]CAD Centre, Nanjing Tech University, Nanjing, Jiangsu 211816, China
[2]Nanjing Tycho Information Technology Company Ltd., Nanjing, Jiangsu 210019, China

Corresponding author: Jingui Lu (lujg@njut.edu.cn)

This work was supported in part by the Technology Innovation Program of the Ministry of Science and Technology of China under Grant 10C26213201084, and in part by Nanjing Tycho Information Technology Company Ltd.

ABSTRACT In the safety protection system of the railway electric multiple unit (EMU), the safety of the running part is extremely important. The daily detection of the internal hazard defects of the wheels in the running parts relies on a professional trackside fault online diagnosis system based on the ultrasonic sensor probe array data. However, the on-line ultrasonic diagnosis of EMU wheels is usually accompanied by various interference noises. The defect echo signals collected by the sensor probe array are weak and are easily submerged by noise, which makes it impossible to perform effective defect identification. This paper proposes an improved threshold function to overcome the discontinuous shortcomings of the classical wavelet soft threshold function and hard threshold function in view of the non-stationary characteristics of the ultrasonic detection signal of the EMU wheels. This paper proposes a sine-type threshold processing function. It is characterized by adopting gradual compression processing to denoise the echo signal of the ultrasonic sensor probe array. In order to verify the validity, the continuity at the threshold is observed through the linear space vector signal, and the algorithm is simulated and tested through the three-dimensional Gaussian echo mathematical model of the ultrasonic signal and the measured ultrasonic envelope signal. Experimental results show that the improved threshold function can suppress the noise in the ultrasonic echo data, improve the signal-to-noise ratio, and retain the waveform characteristics of the defect signal, which is conducive to defect recognition.

INDEX TERMS EMU wheel, fault diagnosis, ultrasonic data, wavelet transform, threshold denoising.

I. INTRODUCTION

In the high-speed rail system [1], [2], wheels are extremely important parts in the running unit of the EMU. The wheels of the EMU play the role of carrying and guiding, and need to bear large static and dynamic loads. Its quality is directly related to the operational safety of high-speed rail. Problems with the wheels may cause wheel collapse, axle cutting, and even vehicle subversion [3], [4]. Wheel status is one of the main factors that affect the safe operation of EMU. At the same time, this is also the focus of the safety inspection of the running unit, the railway management department has to spend a large amount of budget to inspect and maintain the wheels safety every year [5].

At present, the technical route of wheel safety protection is mainly developed from off-line detection mainly based on manual to automatic on-line intelligent detection. The off-line inspection of wheels [6] requires the train to be out of service, and the related parts are disassembled and assembled in the maintenance workshop for non-destructive testing of ultrasonic, electromagnetic, eddy current and other methods [7], [8]. The efficiency of overhaul is low, and the quality of overhaul is subject to operational skills. The overhaul cycle is every hundreds of thousands of kilometers or months, and the daily detection of wheel failures cannot be achieved. The on-line detection method of wheels mainly adopts two types of vehicle-mounted and rail-side, and the method of

The associate editor coordinating the review of this manuscript and approving it for publication was Manuel Rosa-Zurera.

vehicle-mounted detection mainly depends on the monitoring system of multiple temperature and vibration acceleration sensors installed on each bearing [9]. By monitoring the bearing temperature and vibration signals to monitor the bearing and estimate the health of the wheel [10], [11], the system is complex and huge. The trackside system is placed next to the rails and is not directly loaded on the train. It can be placed at some key monitoring stations. In the normal operation state of high-speed trains, the trackside system can monitor thousands of wheels of all passing trains every day [12], [13]. The rail-side system mainly uses electromagnetic ultrasonic [14] and piezoelectric ultrasonic [15] methods, and the electromagnetic ultrasonic method mainly detects wheel surface defects. Piezoelectric ultrasonic method can not only detect wheel surface defects, but also detect deep internal defects through specially designed ultrasonic sensor array [16], which is the main development direction of EMU wheel fault diagnosis methods. Its significance lies in its ability to guarantee the safety of vehicle operation and the personal safety of passengers.

The types of wheel defects are mainly circumferential cracks and radial cracks [17], [18]. According to the technical requirements of the on-line detection system of EMU wheel faults by railway management department, the detection range of wheel faults is circumferential crack and radial crack of the rim, and the corresponding detection sensitivity is respectively the flat bottom ellipse equivalent defect of 40mm for long axis and 30mm for short axis and the transverse hole equivalent defect of $\emptyset 3 \times 100$. The EMU wheel trackside diagnosis system uses the wheel tread as the contact surface between the probe and the wheel. To overcome the shortcomings of small depth of surface wave flaw detection method, the longitudinal wave and transverse wave probes were selected. The reliable coverage method for the main areas where circumferential defects and radial defects occur is to use transverse wave probes with different incidence directions and multiple focusing straight probes to form an ultrasonic sensor array. Longitudinal wave straight probes are sensitive to circumferential defects, and transverse wave probes are sensitive to radial defects. The combination of multiple probes can detect harmful defects. In the actual application, the signal-to-noise ratio of ultrasonic echo data is low [19]. Firstly, due to wheel-rail force, the tread has scratches, peeling and other damages, and the material interface absorbs and spreads attenuation greatly, resulting in weak reflection echo. Secondly, due to the high-speed signal acquisition in the online dynamic process, the ultrasonic echo is often accompanied by various interference waves, mainly manifested as background noise and scattered noise, the echo signal of small defects is weak and easy to be submerged by noise [20]. In addition, the original voltage signal output by the ultrasonic sensor array is extremely weak, so that the weak acoustic signal has a greater degree of attenuation after long-distance transmission. The relatively low signal-to-noise ratio of ultrasound data is a prominent problem, which is not conducive to the determination of damage. Denoising has become an indispensable data processing link in the online trackside diagnosis system for EMU wheel faults.

The ultrasonic sensor array echo signal collected by the wheel rail fault diagnosis system contains both useful defect information and useless interference information. The useless interference signal is mainly noise. Severe noise can cover useful signals, making it difficult to find defects in the echo signal or the judgment of defects is prone to errors, which brings great difficulties to the identification of the signal. To get a true and reliable signal, effective noise suppression methods need to be adopted to improve the signal-to-noise ratio. The traditional methods of denoising wheel ultrasonic data of EMU mainly include linear filtering methods and non-linear filtering methods [21], such as median filtering and Wiener filtering. The disadvantage is that the entropy after signal transformation is increased, the non-stationary characteristics of the signal cannot be characterized, and the signal cannot be achieved. Based on time-frequency domain analysis of short-time Fourier transform [22], [23], Mallat fast algorithm [24], matching pursuit method [25], etc., multiple iterations of noise reduction make the calculation amount very large. Besides, the signal reconstruction method will cause some defect feature information to be lost. To overcome the above shortcomings, based on the analysis of the wheel ultrasonic data and noise characteristics obtained, this paper applies wavelet analysis to the denoising processing of wheel ultrasonic data of EMU. This provides effective data support for the multi-level defect-recognition model integrating micro-features and macro-expert knowledge in the next step.

The main contribution of this paper is to propose a sine-type threshold processing function to improve the traditional soft and hard threshold processing functions of wavelet in view of the non-stationary characteristics of the ultrasonic detection signal of the EMU wheel trackside fault diagnosis system. It is characterized by adopting slow-variation compression processing. As the wavelet coefficients continue to increase, the amount of compression continues to decrease. When the wavelet coefficients are greater than a certain value, no compression processing is performed, so that it can smoothly transition from the soft threshold function to the hard threshold function can better process the noise components in the ultrasonic signal, retain the signal characteristics, improve the signal-to-noise ratio, and facilitate the qualitative identification and analysis of defects.

II. WAVELET DENOISING OF EMU WHEEL ULTRASONIC DATA

A. WAVELET DENOISING PRINCIPLE AND ALGORITHM

Assuming $s(t_i)$ is the original signal, $n(t_i)$ is an independent and identically distributed Gaussian white noise[26] with an expected 0 and a variance of σ^2, then the acquired signal can be expressed as equation (1).

$$f(t_i) = s(t_i) + n(t_i) \quad (i = 1, \ldots, N) \tag{1}$$

It can be known from the linear properties of the wavelet transform that the wavelet coefficient $w_{j,k}$ obtained by the decomposition consists of two parts [27], [28]. One is the wavelet coefficient $u_{j,k}$ corresponding to the signal $s(t_i)$. The other part is the wavelet coefficient $v_{j,k}$ corresponding to the noise $n(t_i)$.

The variance of white noise in binary wavelet transform $W_2^j n(t)$ can be expressed as equation (2) [29], [30].

$$\begin{aligned} E\left[W_2^j n(t)^2\right] &= \int_{-\infty}^{\infty}\int_{-\infty}^{\infty} E[n(u)\, n(v)] \\ &\quad \times \Psi_2^j(t-u)\, \Psi_2^j(\text{t-v})\, du dv \\ &= \int_{-\infty}^{\infty} \sigma^2 \Psi_2^j(t-u)\, du \\ &= \frac{\|\Psi\|^2}{2^j}\sigma^2 \end{aligned} \tag{2}$$

It can be seen from the above formula (2) that as the scale j increases, the mean value of $W_2^j n(t)^2$ decreases, that is, white noise has negative singularity. The maximum modulus of wavelet transform decreases as the scale increases. For the original signal, the maximum value of the wavelet transform modulus increases as the scale increases. It is the change trend of the maximum modulus in the multi-scale space to distinguish signal and noise [31].

B. IMPROVED THRESHOLD PROCESSING FUNCTION

The classical hard and soft threshold denoising methods proposed by Donoho [32], the formula (3) shows the hard threshold function, and the formula (4) shows the soft threshold function, both of which have been widely used in practice and achieved positive results, but both methods have some potential disadvantages. In the hard threshold method, $\hat{w}_{j,k}$ is discontinuous at λ, and the signal reconstructed by $\hat{w}_{j,k}$ will generate some oscillations. In the soft threshold method, although the estimated $\hat{w}_{j,k}$ has overall continuity, when $|w_{j,k}| > \lambda$, there is always a constant deviation between $\hat{w}_{j,k}$ and $w_{j,k}$, which directly affects the degree of approximation between the reconstructed signal and the real signal.

$$\hat{w}_{j,k} = \begin{cases} w_{j,k}, & |w_{j,k}| \geq \lambda \\ 0, & |w_{j,k}| < \lambda \end{cases} \tag{3}$$

$$\hat{w}_{j,k} = \begin{cases} sign\left(w_{j,k}\right), \left(|w_{j,k}| - \lambda\right), & |w_{j,k}| \geq \lambda \\ 0, & |w_{j,k}| < \lambda \end{cases} \tag{4}$$

In order to overcome the shortcomings of soft and hard threshold functions, formula (5) is an improved bivariate wavelet threshold algorithm proposed by Liu *et al.* [33].

$$\hat{w}_{j,k} = \begin{cases} w_{j,k} + \lambda - \dfrac{\lambda}{2\beta+1}, & w_{j,k} < -\lambda \\ sign\left(w_{j,k}\right) \dfrac{\alpha}{(2\beta+1)\lambda^{2\beta}} |w_{j,k}|^{2\beta+1}, & |w_{j,k}| \leq \lambda \\ w_{j,k} - \lambda + \dfrac{\lambda}{2\beta+1}, & w_{j,k} > \lambda \end{cases} \tag{5}$$

where α and β are variable parameters, and β is an integer, which can adjust the order of the transition region.

Although the classic method proposed by Donoho and the threshold function improved by subsequent scholars have achieved positive results for specific engineering applications, in the processing of the EMU wheel fault signal, the hard threshold algorithm only processes wavelet coefficients less than the threshold λ, and the wavelet coefficients greater than the threshold λ also have interference noise. The derivative of the soft threshold algorithm is discontinuous, and there is a deviation between the estimated wavelet coefficient value and the original coefficient, which makes it difficult to distinguish between small singular signals, that is, small defect echo signals and noise. To overcome the shortcomings of classic threshold functions, this paper proposes an improved wavelet threshold algorithm. When the wavelet coefficient is larger than a certain value, the compression process is no longer performed, so that the soft threshold function can be smoothly transitioned to the hard threshold function. The expression defines as equation (6), as shown at the bottom of the next page.

In the formula, μ is a controlling factor and controls $|w_{j,k}| < \lambda$. n is an adjustment factor that adjusts the degree of change in the threshold of $sin\left(\left|\frac{\lambda-\mu}{w_{j,k}}\right|^n \times \frac{\pi}{2}\right)$.

From equation (6), when

$$\mu = 0, \hat{w}_{j,k} = \begin{cases} sign\left(w_{j,k}\right) \\ \times\left[|w_{j,k}| - sin\left(\left|\dfrac{\lambda-\mu}{w_{j,k}}\right|^n \times \dfrac{\pi}{2}\right) \times \lambda\right], & |w_{j,k}| \geq \lambda \\ 0, & |w_{j,k}| < \lambda, \end{cases}$$

when $\mu = \lambda, \hat{w}_{j,k} = \begin{cases} w_{j,k} & |w_{j,k}| \geq \lambda \\ sign\left(w_{j,k}\right) \frac{w_{j,k}^2}{\lambda} & |w_{j,k}| < \lambda \end{cases}$. It can be recognized that the sine-type threshold function is a continuous function like the soft threshold function. This overcomes the problem caused by the discontinuity of the function during hard threshold denoising.

When $w \geq \lambda$, $f(w) = w - sin\left(\frac{\lambda}{w} \times \frac{\pi}{2}\right) \times \lambda$, then when w approaches ∞, $\frac{f(w)}{w} = 1 - \frac{sin\left(\frac{\lambda}{w} \times \frac{\pi}{2}\right) \times \lambda}{w}$ tends to 1. When $w \leq -\lambda$, $f(w) = w + sin\left(\frac{\lambda}{w} \times \frac{\pi}{2}\right) \times \lambda$, then when w approaches $-\infty$, $\frac{f(w)}{w} = 1 + \frac{sin\left(\frac{\lambda}{w} \times \frac{\pi}{2}\right) \times \lambda}{w}$ tends to be 1, so when w increases continuously, $f(w)$ will gradually exhibit the characteristics of a hard threshold function.

When w approaches $\pm\infty$, $f(w) - w$ tends to 0, which means that the sinusoidal threshold function takes $|w_{j,k}| = w_{j,k}$ as the asymptotic line.

In order to intuitively reflect the influence of parameter changes on the improved threshold function, the values of μ and n are respectively taken as $\mu \in [0, \lambda]$ and $n = 3$, and the threshold function graph is drawn with $\mu = \lambda/40$ as the gradient, as shown in Fig. 1.

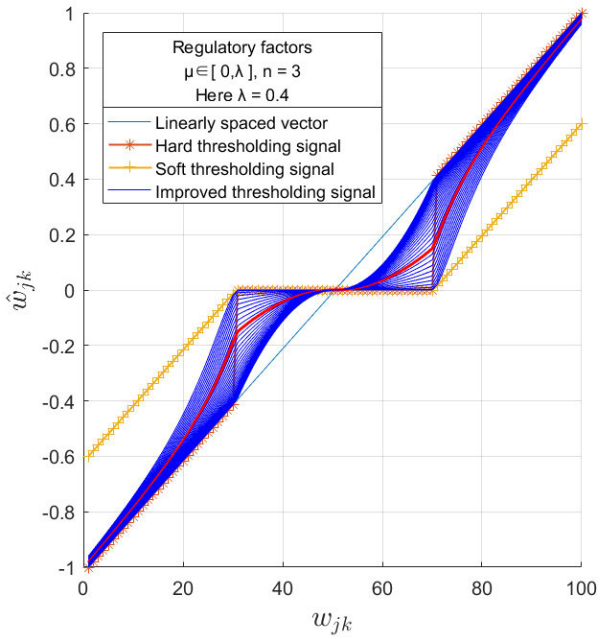

FIGURE 1. Comparison of the effects of three threshold functions on linear space vector processing.

The red line in Fig. 1 is the median curve of the noise reduction function when the parameters $\mu = \lambda/4$ and $n = 3$, taking into account the characteristics of soft and hard threshold functions. When the threshold is constant, the sinusoidal threshold function proposed presents a smooth transition from soft threshold function to hard threshold function near the threshold as μ changes, thus avoiding the problem of oscillations of reconstructed signals caused by discontinuity of the hard threshold method. At the same time, the value of μ directly changes the threshold processing result of wavelet coefficients. This overcomes the disadvantage that the permanent deviation of wavelet coefficients in the soft threshold method leads to the difference between the reconstructed signal and the actual signal. It can be seen that the sinusoidal threshold function proposed in this paper has the characteristics such as continuity, graduality and high - order derivability.

From the above analysis, it can be known that the sinusoidal threshold function combines the advantages of the soft threshold function and the hard threshold function while avoiding the disadvantages of the two.

III. SIMULATION AND EXPERIMENT

A. PERFORMANCE EVALUATION OF ULTRASONIC SENSOR ECHO SIGNAL PROCESSING METHOD

The signal processing method applied to the wheel defect detection of an EMU requires a processed signal with a higher signal-to-noise ratio and less signal distortion [34]. For the evaluation and comparison of denoising results, three indicators of signal-to-noise ratio (SNR), root mean square error (RMSE), and related coefficient (r) are used, which are defined as equations (7) to (9).

$$SNR = 10log_{10}\left|\frac{\sum_n s^2(t)}{\sum_n |f(t) - s(t)|^2}\right| \tag{7}$$

$$RMSE = \sqrt{\frac{1}{n}[f(t) - s(t)]^2} \tag{8}$$

$$r[f(t), s(t)] = \frac{Cov[f(t), s(t)]}{\sqrt{Var[f(t)]\, Var[s(t)]}} \tag{9}$$

Here $f(t)$ is the original signal and $s(t)$ is the denoised signal. Among them, $Cov[f(t), s(t)]$ is the covariance of the original signal $f(t)$ and the denoised signal $s(t)$, and $Var[f(t)]$ is the variance of the original signal $f(t)$, $Var[s(t)]$ is the variance of $s(t)$ after denoising.

The unit of the SNR is decibel (dB). The RMSE and r are dimensionless quantities. The larger the signal-to-noise ratio, the better the denoising effect. The smaller the root mean square error and the higher the related coefficient, the higher the degree of similarity between the denoising signal and the original signal.

B. SIMULATION SIGNAL TEST

According to the mathematical model of the ultrasonic defect echo signal [35], a simulation model of the ultrasonic damage data of the EMU wheels is established as shown in the following equation (10).

$$s(p,t) = \beta exp\left[-b(t-\tau)^2 - \alpha t\right] cos[2\pi f_c(t-\tau) + \varphi] \tag{10}$$

β– Defect reflection coefficient
b– Transducer bandwidth
τ– Delay
α– Attenuation coefficient
f_c– Centre frequency
φ– Initial phase

$$\hat{w}_{j,k} = \begin{cases} w_{j,k} - sin\left(\left|\frac{\lambda-\mu}{w_{j,k}}\right|^n \times \frac{\pi}{2}\right) \times \lambda, & w_{j,k} \geq \lambda \\ \left[1 - sin\left(\left|\frac{\lambda-\mu}{\lambda}\right|^n \times \frac{\pi}{2}\right)\right] \times \frac{w_{j,k}^2}{\lambda}, & 0 < w_{j,k} < \lambda \\ \left[sin\left(\left|\frac{\lambda-\mu}{\lambda}\right|^n \times \frac{\pi}{2}\right) - 1\right] \times \frac{w_{j,k}^2}{\lambda}, & -\lambda < w_{j,k}, < 0 \\ w_{j,k} + sin\left(\left|\frac{\lambda-\mu}{w_{j,k}}\right|^n \times \frac{\pi}{2}\right) \times \lambda, & w_{j,k} \leq -\lambda, \end{cases} , 0 \leq \mu \leq \lambda \tag{6}$$

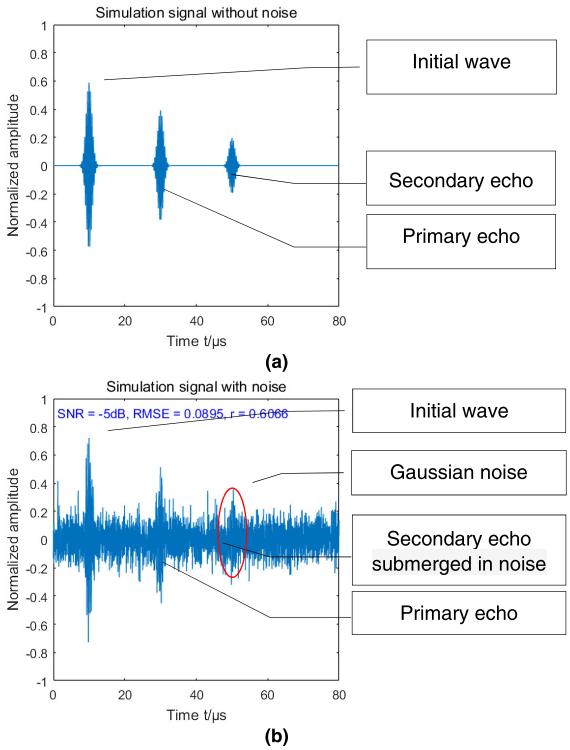

FIGURE 2. Simulation signal.

A set of ultrasonic signals containing a cubic Gaussian echo model with noise added is expressed by equation (11).

$$f(t) = \sum_{i=1}^{3} s(p_i, t) + n(t) \tag{11}$$

The parameters $p = [\beta\ b\ \tau\ \alpha\ f_c\ \varphi]$ are set as listed in equation (12), and $n(t)$ is the additional white Gaussian noise.

$$\begin{cases} p_1 = [0.6\ \ 0.5\ \ 10\ \ 0\ \ 0.75\ \ 0] \\ p_2 = [0.4\ \ 0.5\ \ 30\ \ 0\ \ 0.75\ \ 0] \\ p_3 = [0.4\ \ 0.5\ \ 50\ \ 0\ \ 0.75\ \ 0] \end{cases} \tag{12}$$

The noiseless simulated A-scanning signal is shown in Fig. 2 (a), which is composed of the initial wave, the primary echo, and the secondary echo. The simulated signal with white Gaussian noise is illustrated in Fig. 2 (b), which is superimposed by 5dB noise on the simulation signal. It can be seen in Fig. 2 (b) that the secondary echo is almost submerged in the noise, and its SNR is −5dB, RMSE is 0.0895, and the related coefficient r is 0.6066. Without noise reduction, the secondary ultrasonic echo is difficult to be directly detected.

In this paper, the noise reduction method of EMU wheels based on the damage data and wavelet analysis is used. The processing steps are shown in Fig. 3.

1) DETERMINATION OF WAVELET FUNCTION

Since the useful signals in the ultrasonic detection of EMU wheels are mainly reflected by the sudden change of the signal, the ultrasonic detection signal usually appears as a waveform signal with exponential decay in the time domain. Therefore, the selected wavelet function should have tight support, exponential decay, and symmetry properties in the time domain. In order to obtain the correct detection information, the defect signal in the ultrasonic detection signal is highlighted as much as possible, so the selected wavelet function should have a certain order of vanishing moment.

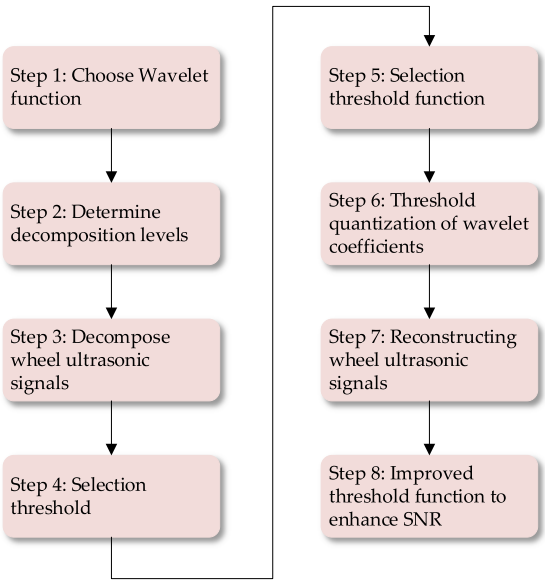

FIGURE 3. Basic steps of wavelet denoising.

Four wavelet functions, sym8, db8, coif2, and bio6.8 are used to process the ultrasonic signals of the EMU wheels. The other denoising parameters are: signal-to-noise ratio −5dB before denoising, 4 layers of decomposition, and heursure threshold criteria, mln threshold adjustment criteria, and soft threshold functions. From the denoising performance indicators in Table 1, it can be seen that using the four wavelet functions of sym8, db8, coif2, and bior6.8, the denoising effect when processing the ultrasonic noise signals of the EMU wheels is better, this article chooses the db8 wavelet function.

TABLE 1. Denoising performance index using four different wavelet functions.

Evaluation index	sym8	db8	coif2	bior6.8
SNR（dB）	1.32	1.6306	1.1778	1.2234
RMSE	0.0492	0.0388	0.0506	0.0527
r	0.9019	0.9422	0.8957	0.8885

2) SELECTION OF THE NUMBER OF DECOMPOSITION LAYERS

According to the multi-resolution theory of wavelet, it can be known that the signal analysis and processing process of wavelet theory are essentially a process of processing wavelet

coefficients at different resolutions or different scales. A signal with a data length of N can theoretically be decomposed into $2logN$ layers, and the data length after each decomposition will be reduced by half. However, each additional level of decomposition level requires a corresponding increase in the amount of calculation and storage space required for one level of decomposition, which does not contribute to engineering practice. Besides, corresponding research points out [36] that before the number of decomposition layers does not reach the ideal number of decomposition layers, the increase in the signal-to-noise ratio is directly related to the increase in the number of layers. However, after reaching a certain number of decomposition levels, the signal-to-noise ratio will no longer increase too much, and in some cases, it will even be greatly decreased. Therefore, it is not appropriate to decompose the signal more from the perspective of the calculation amount, storage amount, or from the perspective of processing effect. Therefore, in the wavelet denoising process of the wheel ultrasonic detection signal, the number of decomposition layers should be appropriately selected. If the number of layers is too low, the effect of improving the signal-to-noise ratio of the processed signal is insufficient. If the number of layers is selected too high, the amount of calculation will increase and the processing effect will be basically unchanged or reduced.

When analyzing the effect of different decomposition layers on the denoising effect of the ultrasonic detection signal, the number of decomposition layers is selected to be 2, 3, 4, 5 and 6, and the other denoising parameters are: signal-to-noise ratio before denoising -5dB, heursure threshold criterion, db8 wavelet basis, mln threshold adjustment criterion, and soft threshold function. The denoising effects of different levels of decomposition are shown in Table 2. It can be seen that the number of decomposition layers directly affect the pros and cons of the denoising effect. When the number of decomposition layers is too small, the noise after denoising is still relatively large. When the number of decomposition layers is too hefty, the amount of calculation will increase, loss of useful information is serious. Therefore, for the ultrasonic detection signal of the EMU wheels, the reasonable number of decomposition layers should be 4 layers, and the comprehensive performance index is optimal at this time.

TABLE 2. Performance index of wavelet denoising using different levels of decomposition.

Evaluation index	2-layer	3-layer	4-layer	5-layer	6-layer
SNR（dB）	1.2633	1.3224	1.4891	1.4815	1.3979
RMSE	0.0689	0.0488	0.0362	0.0447	0.0414
r	0.8539	0.918	0.951	0.9291	0.9465

3) CHOICE OF THRESHOLD

In the process of wavelet denoising, different threshold criteria have different threshold expressions. If threshold λ is too small, the wavelet coefficients will contain too much noise components after applying threshold processing. If threshold λ is too big, the useful signal may be removed, which will cause distortion. The following selects different threshold criteria to compare the denoising effect. Other relevant denoising parameters are: signal-to-noise ratio before denoising is -5dB, db8 wavelet, mln threshold adjustment criterion, and soft threshold function, and the number of decomposition layers is 4 layers.

From the wavelet threshold λ and the denoised signal-to-noise ratio of the different threshold criteria shown in Table 3, it can be seen that the denoising effect using the heursure threshold is better than the rigrsure, sqtwolog and minimaxi threshold criteria, retaining the usefulness of the ultrasonic signal to the maximum section. Therefore, the selection of the heursure threshold is suitable for the analysis and processing of the wheel ultrasonic detection signal.

TABLE 3. Wavelet threshold and SNR using different threshold criteria.

Evaluation index	Threshold criterion			
	rigrsure	sqtwolog	heursure	minimaxi
λ	1.228	6.3419	4.1867	2.7062
SNR（dB）	1.2013	1.3112	1.593	1.411

4) SELECTION OF THRESHOLD PROCESSING FUNCTION

Choosing different threshold processing functions will have a significant effect on the wavelet denoising effect of the ultrasonic detection data. The following are the representative soft and hard threshold functions and the improved threshold processing function described in this article to compare the noise reduction of simulated signals with noises ranging from −5dB to 5dB. The denoising parameters are set as follows: db8 wavelet base, 4-layer decomposition, heursure threshold criterion, mln threshold adjustment criterion, using the signal-to-noise ratio after denoising as an indicator, and compare their effects on ultrasound signals under different noise levels. It can be seen from Fig. 4 that the signal-to-noise ratio of the improved threshold function is higher than the soft and hard threshold functions.

Fig. 5 shows the denoising effect of the soft threshold function, the hard threshold function and the improved threshold function on the noisy signal with a signal-to-noise ratio of −5dB shown in Fig. 2(b). It can be seen from Fig.5(a) and Fig.5(b) that after using the soft threshold function and the hard threshold function to denoise, the noise is removed, but the secondary echo submerged in the noise is lost, and the original signal and the primary echo signal have large distortions. Fig.5(c) shows that after using the improved threshold function to process the noise signal, the secondary echo signal can be effectively detected.

Under the premise of smooth transition between the noise and the signal, the parameters μ and n of this proposed

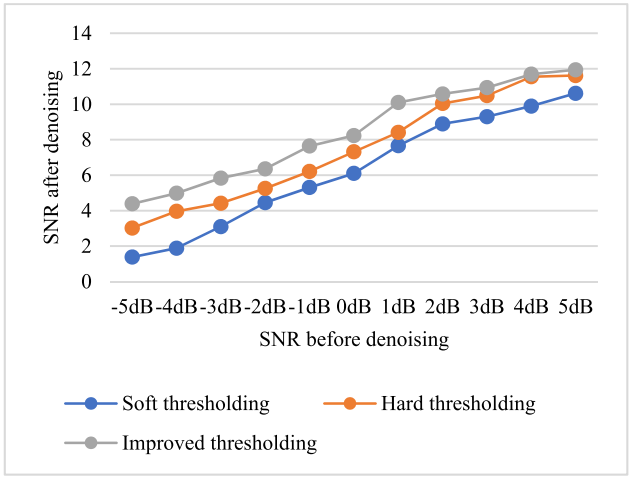

FIGURE 4. Denoising comparison of different SNR signals.

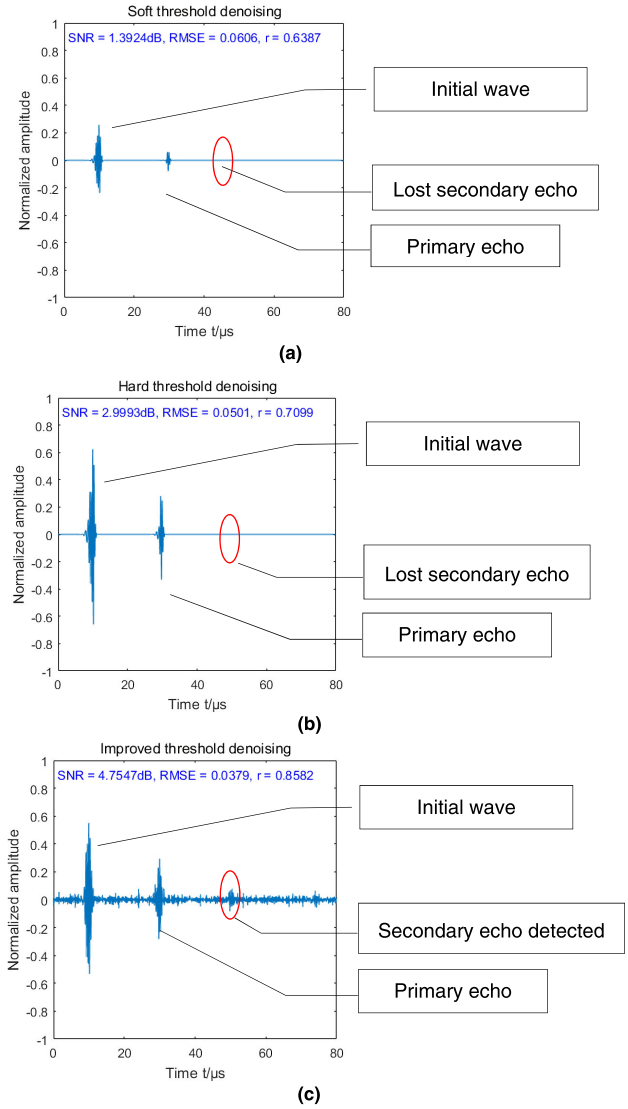

FIGURE 5. Noise reduction effect comparison.

method will affect the noise denoising effect. The optimum denoising effect will be obtained by choosing the appropriate values of μ and n. As shown in Table 4, when $\mu = \lambda/4$ and n= 3, the SNR and related coefficient obtained by the improved threshold algorithm is the largest, and the RMSE of the original signal and the estimated signal is the smallest. The higher the similarity coefficient is, the estimated signal is closer to the original signal, and the denoising effect is better. Compared with the classic soft and hard threshold functions proposed by Donoho, the improved threshold function proposed in this paper can further obtain better denoising performance by adjusting the parameters μ and n.

TABLE 4. Comparison of denoising performance of different threshold functions.

Function		SNR	RMSE	r
Soft threshold		1.3924	0.0606	0.6387
Hard threshold		2.9993	0.0501	0.7099
Improved threshold	$\mu = 0,\ n = 3$	3.2948	0.0492	0.7188
	$\mu = \frac{\lambda}{4}, n = 3$	4.7547	0.0379	0.8582
	$\mu = \frac{\lambda}{2}, n = 3$	4.4046	0.0424	0.7907
	$\mu = \lambda \times \frac{3}{4}, n = 3$	4.3046	0.0434	0.787
	$\mu = \lambda, n = 3$	4.2712	0.0435	0.7867

C. MEASURED SIGNAL TEST

The trackside wheel fault diagnosis system adopts piezoelectric ultrasonic technology to realize the fault detection of moving EMU wheels, the detection process does not require manual intervention, its field application is shown in Fig. 6. The system is mainly composed of probe array units, data acquisition units, data processing module and other parts, as shown in the Fig. 7. The probe array units mainly use the longitudinal wave dual-crystal straight probe with a center frequency of 2.5MHz. The longitudinal wave straight probe is more sensitive to wheel circumferential defects and is mainly

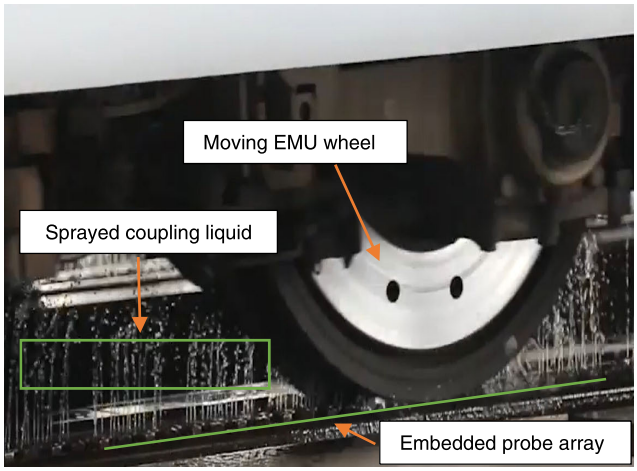

FIGURE 6. Field test of ultrasonic diagnosis of EMU wheels.

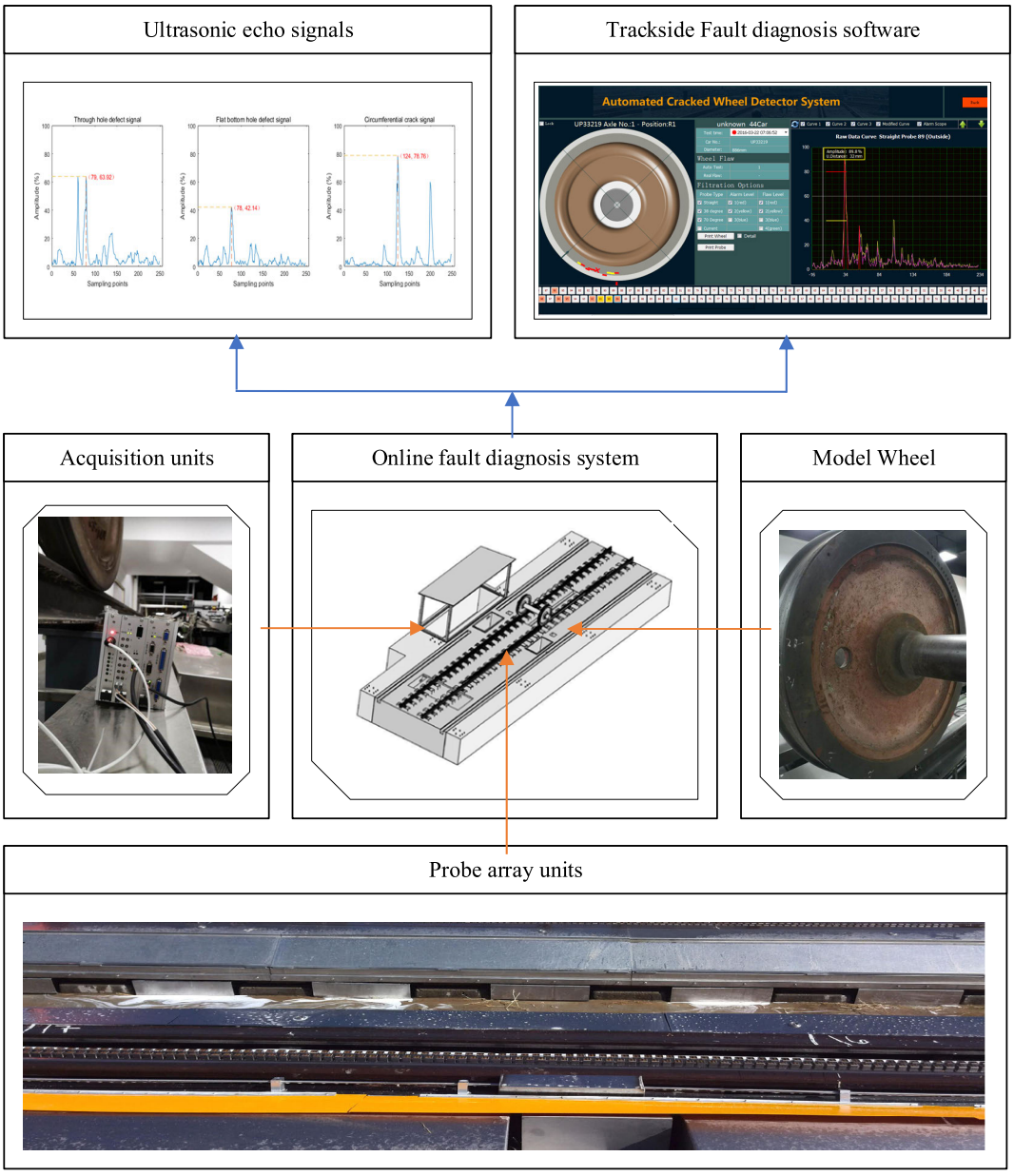

FIGURE 7. Online fault diagnosis system for EMU wheels.

used to detect hazardous cracks inside the EMU wheels. The data acquisition unit excites and collects the ultrasonic signals. After the ultrasonic echo signals are collected by the AD chip with a sampling rate of 80 MHz, they are filtered and compressed. In practical applications, flaw detectors are used to observing the envelope signal to obtain details such as the distance and amplitude of the ultrasonic echo signal. In data processing module, decimation and envelope detection are carried out on the original signal collected at high speed. The data volume is reduced but the signal details are retained. The echo signals are composed of 248 data points. The test data used in the experiments in this paper are multiple sets of data collected by selecting different types of defects on the EMU model wheel shown in Fig. 8 through trackside diagnostic system. The model wheel consists of through hole defect, flat bottom hole defect, and circumferential crack defect. The sample wheel damage is detected by the longitudinal wave method, and the incident angle of the acoustic wave is 0°. The test method is to move the sample wheel through the ultrasonic sensor probe array one by one to measure the three artificial damage defects five times, and obtain a total of 15 measurement samples. According to the above noise reduction method, the ultrasonic sensor probe array signal is preprocessed, the ultrasonic echo envelope signal is shown in Fig. 9, and the noise reduction effect is shown in Fig. 10, Fig. 11 and Fig. 12.

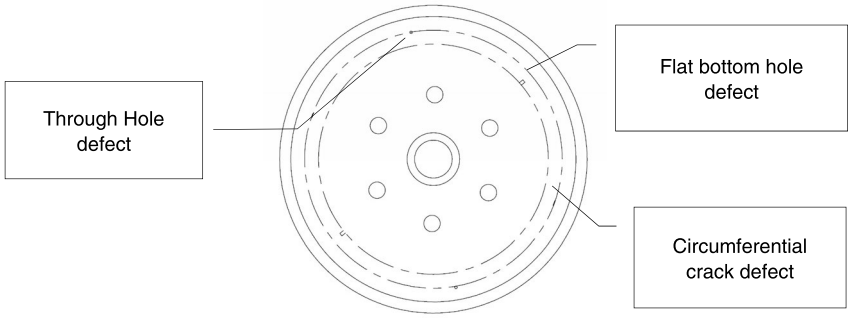

FIGURE 8. Artificial defects of EMU model wheel.

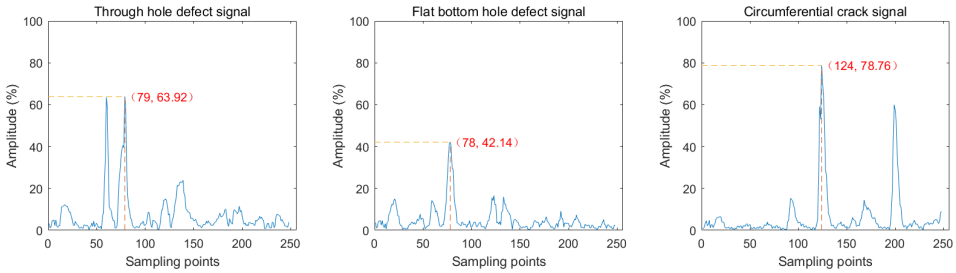

FIGURE 9. Defect echo envelope signal of model wheel.

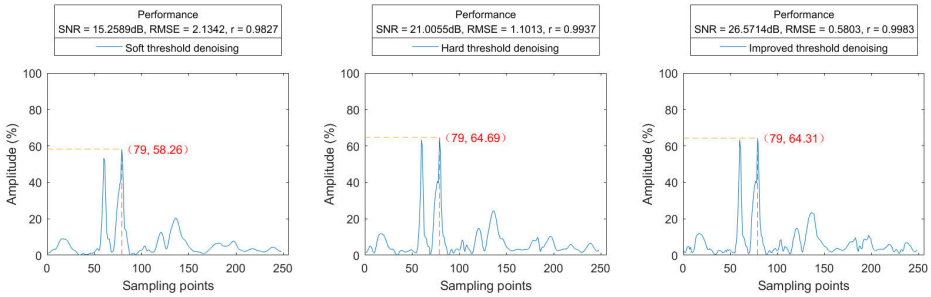

FIGURE 10. Denoising effect of through hole defect.

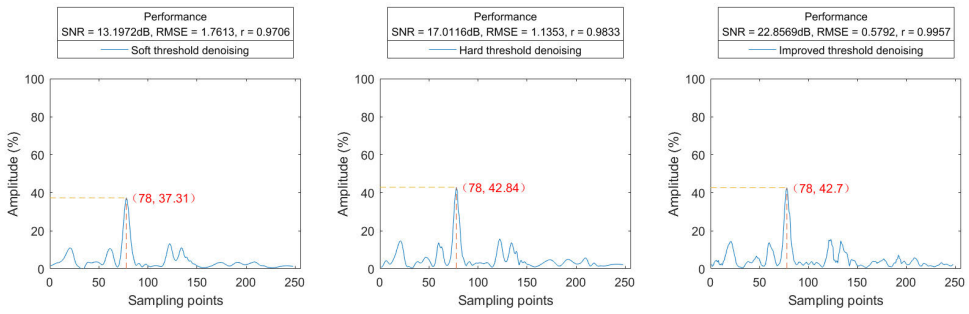

FIGURE 11. Denoising effect of flat bottom hole.

The soft threshold, hard threshold and improved threshold algorithm are used to denoise the measurement samples. Table 5 to Table 7 are the performance evaluation indicators obtained by using soft and hard thresholds and improved threshold methods. In order to compare the noise reduction effect more intuitively, Fig. 13 to 15 are two-dimensional graphs showing the average values of the noise reduction performance evaluation indicators in Tables 5 to 7. It can

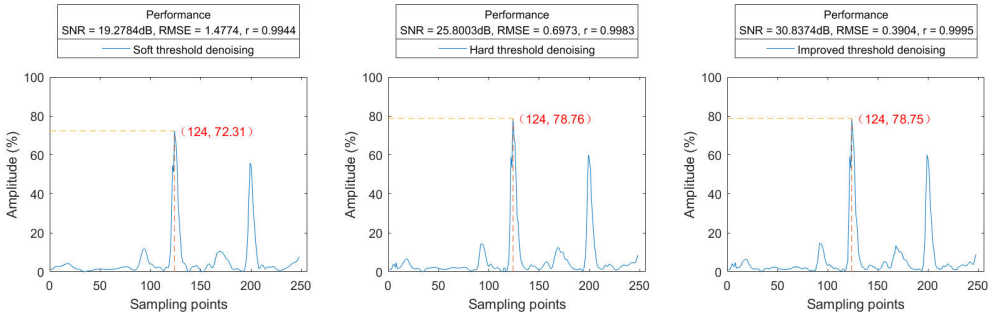

FIGURE 12. Denoising effect of circumferential crack.

TABLE 5. Performance of through-hole defect denoising under different methods.

No.	Soft thresholding			Hard thresholding			Improved thresholding		
	SNR (dB)	RMSE	r	SNR (dB)	RMSE	r	SNR (dB)	RMSE	r
1	15.2589	2.1342	0.9827	21.0055	1.1013	0.9937	26.5714	0.5803	0.9983
2	17.1023	1.7777	0.9893	22.7322	0.9298	0.9959	28.4977	0.4787	0.9989
3	15.5324	2.4051	0.9829	21.0684	1.2716	0.9936	26.7749	0.6592	0.9983
4	13.7455	2.4726	0.9743	17.8805	1.5360	0.9859	23.7632	0.7803	0.9964
5	15.7913	2.1262	0.9840	21.4595	1.1071	0.9939	27.2320	0.5696	0.9984

TABLE 6. Performance of flat bottom hole defect denoising under different methods.

No.	Soft thresholding			Hard thresholding			Improved thresholding		
	SNR (dB)	RMSE	r	SNR (dB)	RMSE	r	SNR (dB)	RMSE	r
1	13.1972	1.7613	0.9706	17.0116	1.1353	0.9833	22.8569	0.5792	0.9957
2	13.0531	1.8893	0.9690	16.9055	1.2125	0.9826	22.5568	0.6326	0.9953
3	14.0547	1.4123	0.9739	17.5382	0.9457	0.9843	23.9305	0.4530	0.9964
4	12.5024	1.6059	0.9624	16.4145	1.0236	0.9788	21.9674	0.5401	0.9942
5	12.8931	1.2627	0.9706	17.6127	0.7333	0.9861	22.7109	0.4078	0.9958

TABLE 7. Performance of circumferential crack defect denoising under different methods.

No.	Soft thresholding			Hard thresholding			Improved thresholding		
	SNR (dB)	RMSE	r	SNR (dB)	RMSE	r	SNR (dB)	RMSE	r
1	19.2784	1.4774	0.9944	25.8003	0.6973	0.9983	30.8374	0.3904	0.9995
2	17.1361	1.7892	0.9904	23.0512	0.9055	0.9966	28.4331	0.4873	0.9990
3	18.6496	1.9883	0.9934	24.4670	1.0177	0.9977	29.5968	0.5638	0.9993
4	19.4481	2.4482	0.9942	26.1336	1.1339	0.9984	31.8480	0.5873	0.9996
5	17.8851	2.1845	0.9923	23.6555	1.1242	0.9972	29.2337	0.5915	0.9992

be seen that the performance evaluation indexes obtained by using the improved threshold method for defects are the best, which are represented by the highest signal-to-noise ratio, the smallest root mean square error, and the largest similarity coefficient. In addition, it can be seen from the time-domain Fig. 10 to Fig. 12 and Table 8 that the peak center position and amplitude characteristics of the noise reduction signal obtained after the improved threshold method are compared with the signal before noise reduction, the defect peak center position does not change, and the defect amplitude characteristics are almost the same, with the lowest deviation rate, which will not affect the qualitative and quantitative evaluation of defects. In summary, the three threshold methods can improve the signal-to-noise ratio and the resolution

TABLE 8. Peak coordinate values comparison under different threshold functions.

Defect type	Peak coordinates	Original echo envelope signal value	Soft threshold denoising signal		Hard threshold denoising signal		Improved threshold denoising signal	
			Value	Deviation rate	Value	Deviation rate	Value	Deviation rate
Through Hole	Peak center	79	79	0.00%	79	0.00%	79	0.00%
	Amplitude	63.92	58.26	-8.85%	64.69	1.20%	64.31	0.61%
Flat bottom hole	Peak center	78	78	0.00%	78	0.00%	78	0.00%
	Amplitude	42.14	37.31	-11.46%	42.84	1.66%	42.7	1.33%
Circumferential crack	Peak center	124	124	0.00%	124	0.00%	124	0.00%
	Amplitude	78.76	72.31	-8.19%	78.76	0.00%	78.75	-0.01%

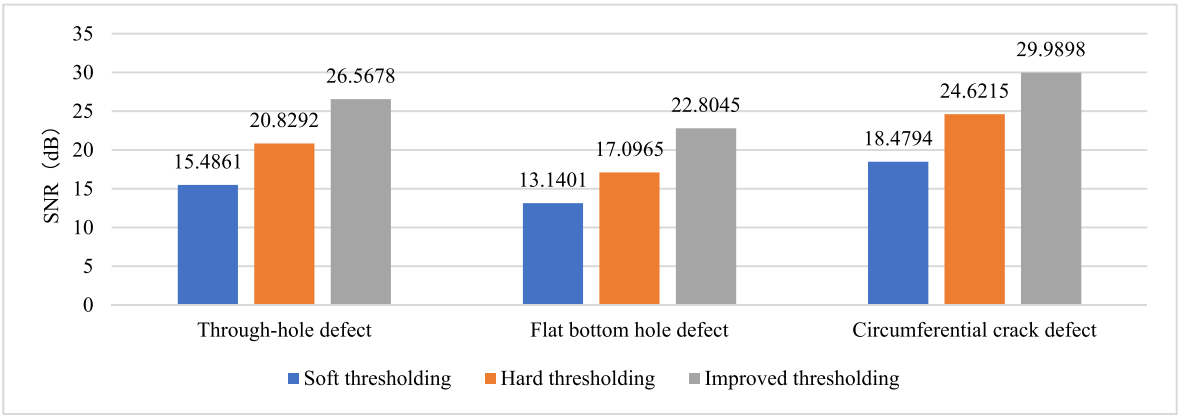

FIGURE 13. SNR comparison of different threshold function denoising.

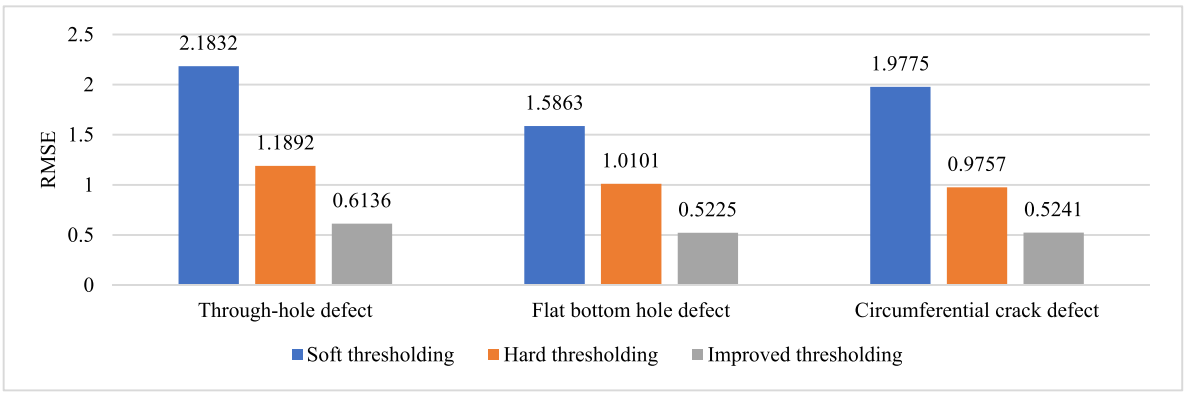

FIGURE 14. RMSE comparison of different threshold function denoising.

of the signal, but the improved threshold method has better performance.

IV. DISCUSSION

The experimental results show that both the classical soft and hard threshold functions proposed by Donoho and the sinusoidal threshold functions presented in equation (6) in this paper can suppress noise. Compared with the hard threshold and the soft threshold function, both the bivariate wavelet threshold function mentioned in equation (5) and the sinusoidal threshold function proposed in equation (6) add a smooth transition region within the critical threshold, which makes the new threshold function have such characteristics as continuity, graduality and high-order differentiability. Table 9 shows the average denoising signal-to-noise ratio index of the two functions in equation (5) and (6). It can be seen that the threshold function of equation (6) has enhanced SNR index than that of equation (5).

In the wavelet domain, the improved threshold function improves the discontinuity of the hard threshold function, which can make the signal after denoising using the new threshold function relatively smooth, and retain the original signal edge characteristics. In the measured echo signal of the wheel ultrasonic sensor array, the signal-to-noise ratio is often low due to factors such as material interface absorption and propagation attenuation. Through the improved wavelet threshold function to reduce noise, it can effectively ensure that the time domain peak center position and amplitude

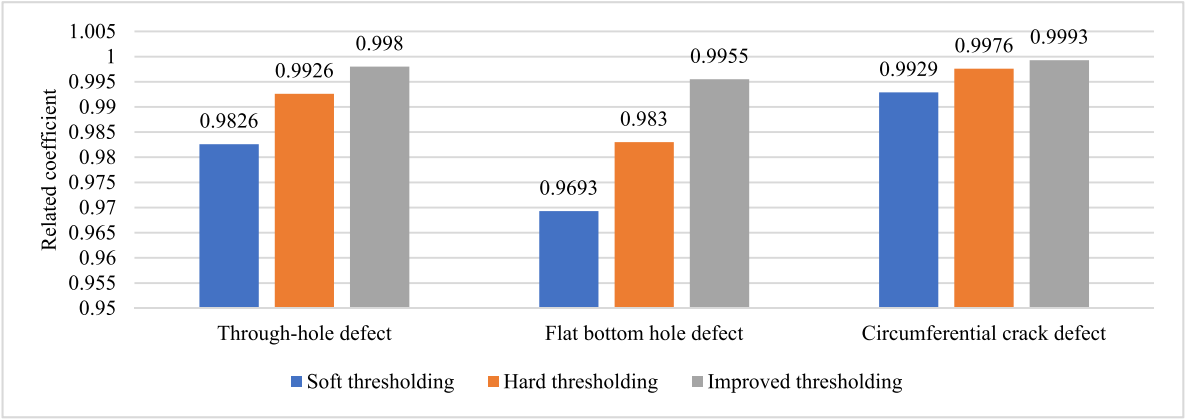

FIGURE 15. Related coefficient comparison of different threshold function denoising.

TABLE 9. SNR comparison under different improved threshold functions.

Defect type	SNR of bivariate wavelet threshold function denoising (equation 5)	SNR of sinusoidal threshold function denoising (equation 6)
Through Hole	23.3475	26.5678
Flat bottom hole	19.8995	22.8045
Circumferential crack	27.0281	29.9898

remain unchanged. The improved signal-to-noise ratio is not only conducive to defect location and quantification, but also conducive to the extraction of time-frequency features and defect characterization [37] of subsequent ultrasonic signals.

In the field of ultrasonic nondestructive testing, defect positioning, quantitative and qualitative assessment are the three key issues [38]. Many experimental studies have made great progress in locating and quantifying defects, and are constantly maturing and improving. However, due to the different nature, orientation, geometry, surface roughness, and inclusions of the defect, the reflection characteristics of the defect to ultrasonic waves are also different. In addition, the characteristics of the detection system used will also affect the reflection characteristics of the defect to ultrasonic waves. It shows that the ultrasonic response of defects obtained by ultrasonic inspection is a comprehensive response, which makes the characterization of defects a difficult problem. So far, due to the complexity of the actual ultrasonic sensor array sound field, the signal-to-noise ratio of the ultrasonic signal is relatively low. For a specific complex background and high-speed operation equipment such as the EMU wheel fault trackside diagnostic system, better defect positioning, quantitative and qualitative should be performed. The effective preprocessing of ultrasonic data, such as effective acoustic signal recognition and noise removal, still needs further study.

V. CONCLUSION

According to the prominent noise problem in the application of trackside ultrasonic damage data of EMU wheels, combined with the distribution characteristics of noise in the time-frequency domain and the advantages of wavelet soft and hard threshold denoising methods, an improved threshold function is proposed. The linear space vector processing results show that adjusting the values of μ and n by the improved threshold function can make the improved threshold function flexibly change between hard and soft thresholds. The appropriate adjustment value enables the improved threshold function to retain the high frequency part of the useful signal during threshold processing, which is better to suppress the signal oscillation phenomenon. The noise reduction results of the simulated signal and the measured signal show that the improved threshold function improves the signal-to-noise ratio compared with the soft threshold function and the hard threshold function, while further reducing the root mean square error and has a higher similarity coefficient. The improved threshold function is easy to implement in engineering applications, which provides favorable conditions for intelligent diagnosis of EMU wheel defects through damage morphological data.

ACKNOWLEDGMENT

The authors are thankful to the colleagues from the CAD Centre, Nanjing Tech University, and Nanjing Tycho Information Technology Company Ltd., who provided support in the in-situ test.

CONFLICTS OF INTEREST

The authors declare no conflict of interest.

REFERENCES

[1] M. A. Spiroiu and M. Nicolescu, "Failure modes analysis of railway wheel," in *Proc. MATEC Web Conf.*, vol. 178, 2018, p. 6005.

[2] G. Zhang and R. Ren, "Study on typical failure forms and causes of high-speed railway wheels," *Eng. Failure Anal.*, vol. 105, pp. 1287–1295, Nov. 2019.

[3] H. Hu, B. Tang, X. Gong, W. Wei, and H. Wang, "Intelligent fault diagnosis of the high-speed train with big data based on deep neural networks," *IEEE Trans. Ind. Informat.*, vol. 13, no. 4, pp. 2106–2116, Aug. 2017.
[4] Y. Li, M. J. Zuo, J. Lin, and J. Liu, "Fault detection method for railway wheel flat using an adaptive multiscale morphological filter," *Mech. Syst. Signal Process.*, vol. 84, pp. 642–658, Feb. 2017.
[5] S. S. Artagan, L. B. Ciampoli, F. D'Amico, A. Calvi, and F. Tosti, "Non-destructive assessment and health monitoring of railway infrastructures," *Surv. Geophys.*, vol. 41, no. 3, pp. 447–483, May 2020.
[6] M. Sasidharan, M. P. N. Burrow, and G. S. Ghataora, "A whole life cycle approach under uncertainty for economically justifiable ballasted railway track maintenance," *Res. Transp. Econ.*, vol. 80, May 2020, Art. no. 100815.
[7] D. F. C. Peixoto and P. M. S. T. de Castro, "Fatigue crack growth of a railway wheel," *Eng. Failure Anal.*, vol. 82, pp. 420–434, Dec. 2017.
[8] C. Zhou, L. Gao, H. Xiao, and B. Hou, "Railway wheel flat recognition and precise positioning method based on multisensor arrays," *Appl. Sci.*, vol. 10, no. 4, p. 1297, Feb. 2020.
[9] N. Bosso, A. Gugliotta, and N. Zampieri, "Wheel flat detection algorithm for onboard diagnostic," *Measurement*, vol. 123, pp. 193–202, Jul. 2018.
[10] A. Alemi, F. Corman, Y. Pang, and G. Lodewijks, "Evaluation of the influential parameters contributing to the reconstruction of railway wheel defect signals," *Proc. Inst. Mech. Eng., F, J. Rail Rapid Transit*, vol. 234, no. 9, pp. 1005–1016, Oct. 2020.
[11] G. Krummenacher, C. S. Ong, S. Koller, S. Kobayashi, and J. M. Buhmann, "Wheel defect detection with machine learning," *IEEE Trans. Intell. Transp. Syst.*, vol. 19, no. 4, pp. 1176–1187, Apr. 2018.
[12] M. Asplund, M. Palo, S. Famurewa, and M. Rantatalo, "A study of railway wheel profile parameters used as indicators of an increased risk of wheel defects," *Proc. Inst. Mech. Eng., F, J. Rail Rapid Transit*, vol. 230, no. 2, pp. 323–334, Feb. 2016.
[13] X.-Z. Liu, C. Xu, and Y.-Q. Ni, "Wayside detection of wheel minor defects in high-speed trains by a Bayesian blind source separation method," *Sensors*, vol. 19, no. 18, p. 3981, Sep. 2019.
[14] J. Huo, Z. Liu, J. Xiao, P. Zhao, and Y. Li, "Development of online electromagnetic tomography demodulation system for rail defect inspection," in *Proc. IEEE SENSORS*, Oct. 2018, pp. 1–4.
[15] F. Honarvar and A. Varvani-Farahani, "A review of ultrasonic testing applications in additive manufacturing: Defect evaluation, material characterization, and process control," *Ultrasonics*, vol. 108, Dec. 2020, Art. no. 106227.
[16] D. X. Hua, S. Z. Ying, and M. J. Song, "Overview of an automated ultrasonic wheel defect detection technology," in *Proc. ASNT Annu. Conf.*, 2016, pp. 22–29.
[17] A. Alemi, F. Corman, and G. Lodewijks, "Condition monitoring approaches for the detection of railway wheel defects," *Proc. Inst. Mech. Eng., F, J. Rail Rapid Transit*, vol. 231, no. 8, pp. 961–981, Sep. 2017.
[18] N. Montinaro, G. Epasto, D. Cerniglia, and E. Guglielmino, "Laser ultrasonics inspection for defect evaluation on train wheel," *NDT E Int.*, vol. 107, Oct. 2019, Art. no. 102145.
[19] Q. Ailing, B. Bingwen, and Z. Guangming, "Ultrasonic signal denoising technology based on SMP algorithm," *J. Phys., Conf. Ser.*, vol. 1550, May 2020, Art. no. 022012.
[20] X. Bai, B. Tie, J.-H. Schmitt, and D. Aubry, "Finite element modeling of grain size effects on the ultrasonic microstructural noise backscattering in polycrystalline materials," *Ultrasonics*, vol. 87, pp. 182–202, Jul. 2018.
[21] B. L. Rozovsky and S. V. Lototsky, *Stochastic Evolution Systems: Linear Theory and Applications to Non-Linear Filtering*, vol. 89. Springer, 2018.
[22] C. Mateo and J. A. Talavera, "Short-time Fourier transform with the window size fixed in the frequency domain," *Digit. Signal Process.*, vol. 77, pp. 13–21, Jun. 2018.
[23] L. Li, H. Cai, H. Han, Q. Jiang, and H. Ji, "Adaptive short-time Fourier transform and synchrosqueezing transform for non-stationary signal separation," *Signal Process.*, vol. 166, Jan. 2020, Art. no. 107231.
[24] S. Mallat and W. L. Hwang, "Singularity detection and processing with wavelets," *IEEE Trans. Inf. Theory*, vol. 38, no. 2, pp. 617–643, Mar. 1992.
[25] N. Ruiz-Reyes, P. Vera-Candeas, J. Curpián-Alonso, R. Mata-Campos, and J. C. Cuevas-Martínez, "New matching pursuit-based algorithm for SNR improvement in ultrasonic NDT," *NDT E Int.*, vol. 38, no. 6, pp. 453–458, Sep. 2005.
[26] W. Feng, X. Zhou, X. Zeng, and C. Yang, "Ultrasonic flaw echo enhancement based on empirical mode decomposition," *Sensors*, vol. 19, no. 2, p. 236, Jan. 2019.
[27] Y. Cui, S. Chen, M. Qu, and S. He, "Research and application of new threshold de-noising algorithm for monitoring data analysis in nuclear power plant," *J. Shanghai Jiaotong Univ.*, vol. 22, no. 3, pp. 355–360, Jun. 2017.
[28] Z. Gan, F. Zou, N. Zeng, B. Xiong, L. Liao, H. Li, X. Luo, and M. Du, "Wavelet denoising algorithm based on NDOA compressed sensing for fluorescence image of microarray," *IEEE Access*, vol. 7, pp. 13338–13346, 2019.
[29] D. Zhang, "Wavelet transform," in *Fundamentals of Image Data Mining*. Springer, 2019, pp. 35–44.
[30] M. Rhif, A. Ben Abbes, I. Farah, B. Martínez, and Y. Sang, "Wavelet transform application for/in non-stationary time-series analysis: A review," *Appl. Sci.*, vol. 9, no. 7, p. 1345, Mar. 2019.
[31] X. Xu, M. Luo, Z. Tan, and R. Pei, "Echo signal extraction method of laser radar based on improved singular value decomposition and wavelet threshold denoising," *Infr. Phys. Technol.*, vol. 92, pp. 327–335, Aug. 2018.
[32] D. L. Donoho, "De-noising by soft-thresholding," *IEEE Trans. Inf. Theory*, vol. 41, no. 3, pp. 613–627, May 1995.
[33] H. Liu, W. Wang, C. Xiang, L. Han, and H. Nie, "A de-noising method using the improved wavelet threshold function based on noise variance estimation," *Mech. Syst. Signal Process.*, vol. 99, pp. 30–46, Jan. 2018.
[34] M. Srivastava, C. L. Anderson, and J. H. Freed, "A new wavelet denoising method for selecting decomposition levels and noise thresholds," *IEEE Access*, vol. 4, pp. 3862–3877, 2016.
[35] G. Cardoso and J. Saniie, "Data compression and noise suppression of ultrasonic NDE signals using wavelets," in *Proc. IEEE Symp. Ultrason.*, vol. 1, Oct. 2003, pp. 250–253.
[36] F. M. Bayer, A. J. Kozakevicius, and R. J. Cintra, "An iterative wavelet threshold for signal denoising," *Signal Process.*, vol. 162, pp. 10–20, Sep. 2019.
[37] K. Albindo, C. Ng, T. Ng, and W. Chia, "Characterization of train fleet wheel condition in a metro," in *Noise and Vibration Mitigation for Rail Transportation Systems*. Springer, 2018, pp. 747–758.
[38] S. K. Dwivedi, M. Vishwakarma, and P. A. Soni, "Advances and researches on non destructive testing: A review," *Mater. Today: Proc.*, vol. 5, no. 2, pp. 3690–3698, 2018.

ZHILIN SUN was born in 1978. He received the M.S. degree from Nanjing Tech University, Nanjing, China, in 2009, where he is currently pursuing the Ph.D. degree in mechanical engineering.

From 2009 to 2020, he was an Engineer with Nanjing Tycho Information Technology Company Ltd. (a professional research unit for trackside inspection equipment), China. His current research interests include the mechanical fault diagnosis and prediction, and intelligent optimization algorithm.

JINGUI LU was born in 1966. He received the M.S. degree from the Harbin Institute of Technology, Harbin, China, in 1990, and the Ph.D. degree in mechanical engineering from the Huazhong University of Science and Technology, Wuhan, China, in 1994.

From 1994 to 1996, he engaged in postdoctoral research at the Postdoctoral Station of Aeronautics and Astronautics Engineering, Nanjing University of Aeronautics and Astronautics. In 1997, he engaged in collaborative research at the Institute of Science and Technology, Tokyo Institute of Technology. In 2007, he conducted collaborative research at Utah State University. Since 1998, he has been a Professor with the CAD Centre, Nanjing Tech University. As the Chief Editor, he has participated in the compilation of four academic works. More than 60 academic articles have been published in domestic and foreign journals and conferences. His current research interests include intelligent optimization algorithm and intelligent technology in information engineering.